

Absence of entanglement transition due to measurement-induced skin effect

Yu-Peng Wang,^{1,2} Chen Fang,^{1,3,4,*} and Jie Ren^{1,2,†}

¹*Beijing National Laboratory for Condensed Matter Physics and Institute of Physics,
Chinese Academy of Sciences, Beijing 100190, China*

²*University of Chinese Academy of Sciences, Beijing 100049, China*

³*Songshan Lake Materials Laboratory, Dongguan, Guangdong 523808, China*

⁴*Kavli Institute for Theoretical Sciences, Chinese Academy of Sciences, Beijing 100190, China*

A quantum many-body system subject to unitary evolution and repeated local measurements with an increasing rate undergoes an entanglement transition from (sub)extensive to area law entropy scaling. We find that certain open boundary systems under “generalized monitoring” display an anomalous late-time particle concentration on the edge, reminiscent of the “skin effect” in non-Hermitian systems. Such measurement-induced skin effect will suppress the entanglement generation, rendering the system short-range entangled without any entanglement transition.

The competition between the measurement and unitary evolution produces a novel *measurement-induced phase transition* (MIPT) [1–11], where a random quantum circuit [12–16] interspersed by onsite measurements with an increasing rate goes from a volume-law regime to an area-law regime. Similar entanglement transitions also appear in the context of monitored fermions [17–25], monitored open systems [26, 27], circuits with pure measurements [28, 29], random tensor networks [30–33], and quantum error correction thresholds [34–37]. Measurements introduce intrinsic randomness to the otherwise deterministic dynamics, with each set of recorded measurement results corresponding to a specific trajectory [38]. Among various frameworks trying to explain the MIPT [18, 25, 34–37, 39–46], one approach focuses on a specific trajectory, of which the evolution is described by a non-Hermitian Hamiltonian, where the entanglement transition in some systems coincides with the spontaneous *PT* symmetry breaking [47–51].

One unique phenomenon in certain non-Hermitian open boundary systems is the *non-Hermitian skin effect* [52–59], where a finite portion of the eigenstates are spatially concentrated on the edges. Dynamically, the skin effect implies that the late-time state from the quench dynamics will have particles concentrated near the edges. The Pauli exclusion principle predicts a nearly tensor-product structure of the steady state which obeys the area-law entanglement scaling, suggesting the absence of MIPT and seemingly contradicting the putative universal entanglement transition in the monitored systems. However, this simple argument assumes that the particular non-Hermitian evolution captures the entanglement behavior of the whole ensemble of trajectories, which is generally not guaranteed. Indeed, we will show in this work that for systems under “projective monitoring” (the exact definition of which will be given later), there will be no skin effect in the trajectory-averaged dynamics. A natural question is whether the skin effect can appear in the whole ensemble of trajectories and thus suppress the entanglement transition.

In this letter, we answer the question positively by considering a generalized version of monitoring. The central result is the discovery of a measurement-induced skin effect (MISE) in the generalized monitored fermionic open boundary systems. We introduce an extensive local order parameter, the classical entropy, which not only characterizes the skin effect but also imposes an upper bound on the bipartite entanglement entropy. Numerical simulations of finite-size open boundary systems show a scale invariance of the classical entropy, which implies the saturation of the entanglement entropy in the thermodynamics limit at arbitrarily small measurement rates. The scaling property persists even when the interaction is turned on, therefore eliminating (sub)extensive entangled phases believed to appear in the weakly-monitored regime. Besides, MISE also gives a many-body version of the skin effect, which is numerically tractable due to the suppression of entanglement, and which, in principle, can be experimentally realized without exponential overheads.

Projective monitoring.— A standard quantum measurement process is formulated as a set of complete projectors $\{P_m\}$, with each m representing a distinct outcome. Measurement on a state $|\psi\rangle$ produces a probabilistic distribution of m according to Born rule: $p_m = \|P_m|\psi\rangle\|^2$, and after which the state becomes $P_m|\psi\rangle/p_m$. When the unitary evolution is described by a Hamiltonian, we usually consider a coarse-grained version of the hybrid dynamics called the *projective monitoring* [60], formulated as the *stochastic Schrödinger equation* (SSE) [61–63]:

$$d|\psi\rangle = -iH_{\text{eff}}|\psi\rangle dt + \sum_m \left[\frac{P_m|\psi\rangle}{\|P_m|\psi\rangle\|} - |\psi\rangle \right] dW_m, \quad (1)$$

where the effective non-Hermitian Hamiltonian is $H_{\text{eff}} = H - \frac{i\gamma}{2} \sum_m P_m$ in which H is the Hamiltonian and γ the measurement rate. Each dW_m is an independent Poisson random variable taking the discrete values 0 or 1. For a small interval Δt , the probability for $dW_m = 1$ (meaning the probe registers a quantum jump) is proportional to

$\gamma\Delta t$ [60]. If there are exponentially many experiments carried out from which we select a trajectory with no jump registered, this *post-selected* evolution is described by H_{eff} .

When considering the whole ensemble of trajectories, the averaged dynamics of Eq. (1) is equivalently described in the density matrix formalism by the Lindblad master equation [64–66]:

$$\frac{d}{dt}\rho = -i[H, \rho] - \frac{\gamma}{2} \sum_m \{L_m^\dagger L_m, \rho\} + \gamma \sum_m L_m \rho L_m^\dagger, \quad (2)$$

where $\rho = |\psi\rangle\langle\psi|$ obtained by averaging over all trajectories, and $L_m = P_m$ is called the *jump operator*. One can prove that Eq. (2) in general leads to a homogeneous nonequilibrium steady state ρ_{NESS} , i.e., $\frac{d}{dt}\rho_{\text{NESS}} = 0$ and $\text{Tr}[n_i \rho_{\text{NESS}}] = \nu$ (where ν is the filling number). To see this, we first note that for the projective monitored dynamics, all jump operators $\{P_i\}$ are Hermitian. The maximally mixed state within a given particle-number sector $\rho = \mathbb{I}_\nu$ (the subscript indicates the subspace spanned by the states of filling number ν) is automatically a steady state for Eq. (2). In addition, ρ_{NESS} for generic Lindblad equation is nondegenerate [67–70]. That is, even if we encounter an accidental degeneracy of ρ_{NESS} , we can usually find a suitable boundary perturbation to break the degeneracy. For the specific model studied in this work, we prove the uniqueness of ρ_{NESS} in the Supplemental Material [60]. Therefore, we exclude the possibility of the skin effect in the case of projective monitoring.

Generalized monitoring.— Notably, projective monitoring is an idealized approximation of an actual measurement process. Physically, detecting a quantum state requires a probe interacting with the system, which will inevitably disturb the measured states. Formally, the generalized measurement is formulated as the *positive operator-valued measure* [71, 72]. The continuous version of the generalized measurement, often denoted as the *generalized monitoring*, is still formulated as the SSE in Eq. (1), with the projector P_m replaced by a general operator L_m . The evolution of the density matrix is also described by Eq. (2). In this study, we focus on a particular form of SSE where $L_m = U_m P_m$ corresponds to adding a unitary feedback operator U_m to the projective monitoring process. The conditional feedback does not affect the effective non-Hermitian Hamiltonian H_{eff} but instead operates on those trajectories that deviated from the post-selected trajectory.

Notably, although Eq. (2) is equivalent to Eq. (1) when considering particle density evolution, the inclusion of feedback renders Eq. (2) non-integrable and thus computationally inaccessible. Nonetheless, by taking the trajectory average, the stochastic evolution of Eq. (1) provides an efficient numerical method [60] for the dynamics of the observables (or entanglement), as long as U_i preserves the Gaussian state structure [73]. Thus in the follow-

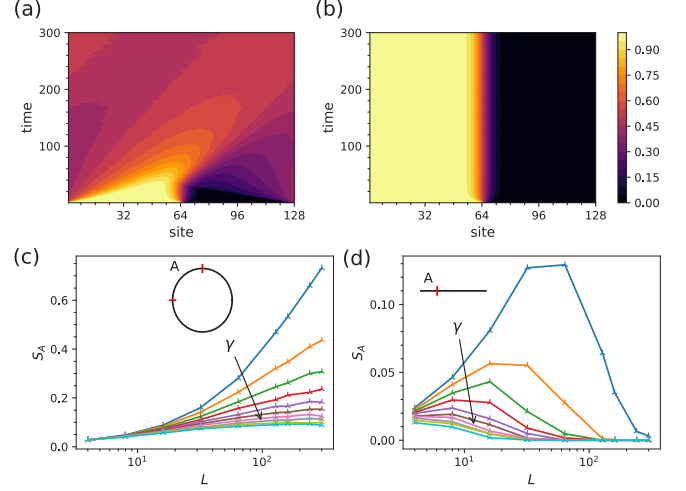


FIG. 1. Simulation of the monitored free fermion model with feedback $U_i = \exp(i\pi n_{i+1})$. (a)(b) Trajectory-averaged dynamics of onsite particle density, starting from a half-filled product state $|1 \dots 10 \dots 0\rangle$. The system size is $L = 128$, the measurement rate $\gamma = 0.3$, and the time span $(0, 300)$. (a) Under periodic boundary conditions, the density eventually disperses to a homogeneous distribution, while (b) the steady-state displays strong particle localization under open boundary conditions. (c)(d) Scaling of steady-state entanglement entropy $S(L/4)$, with $\gamma = \{0.1, 0.2, 0.3, 0.4, 0.5, 0.6, 0.7, 0.8, 0.9, 1.0\}$ increasing along the arrow. (c) Under periodic boundary conditions, the entropy scaling shows a transition from subextensive logarithmic growth to an area law, while (d) under open boundary conditions, the entropies first increase for small system size, since the domain wall regions cross the $L/4$ cuts. For large enough system sizes, the $L/4$ cuts locate deeply in the static domain, therefore the entropies approach zeroes, and no entanglement transition happens.

ing of this letter, we carry out the numerical simulation primarily based on SSE.

Measurement-induced skin effect.— We first consider the a spinless fermion chain with nearest-neighbor hopping Hamiltonian: $H = \sum_i (c_i^\dagger c_{i+1} + c_{i+1}^\dagger c_i)$. The generalized monitoring consists a projector $P_i = \frac{1}{2}(c_i^\dagger - ic_{i+1}^\dagger)(c_i + ic_{i+1})$ acting on two adjacent sites, and a conditional unitary feedback $U_i = \exp(i\theta n_{i+1})$. The effective non-Hermitian Hamiltonian $H_{\text{eff}} = \sum_i [t_L c_i^\dagger c_{i+1} + t_R c_{i+1}^\dagger c_i - \mu(n_i + n_{i+1})]$, where $t_{L/R} = 1 \pm \gamma/4$ and $\mu = i\gamma/4$, is the Hatano-Nelson model [74] displaying non-Hermitian skin effect. The observable being monitored is the occupation number of a local quasimode created by $d^\dagger = c_i^\dagger - ic_{i+1}^\dagger$. In the momentum space, $d^\dagger = \sum_k f(k) c_k^\dagger$ where $|f(k)|^2 = \frac{1}{2}(1 + \sin k)$, meaning that this quasimode is a right-moving wave packet. The post-selected evolution corresponds to the trajectory where no such mode is detected, leaving the left-moving mode probabilistically favored. In the projective monitoring case, the detected right-moving quasimodes will

balance out the momentum distribution, leaving a steady state of homogeneity.

We show for this free fermion model that the balance of particle distribution will be broken by the nontrivial feedback U_i , which is temporarily fixed as a $(\theta = \pi)$ -phase gate at site $(i + 1)$ since the system shows the strongest skin effect at this setup. The π -phase feedback will convert the detected d^\dagger mode to $\tilde{d}^\dagger = c_i^\dagger + ic_{i+1}^\dagger$, which is a left-moving quasimode. The generalized monitoring thus always increases left-moving particles, resulting in the MISE where particles concentrate on the boundary.

As displayed in Fig. 1b, for an open boundary system starting from the half-filled product state $|\psi_0\rangle = |1 \cdots 10 \cdots 0\rangle$, the late-time dynamics still features two static domains where $\langle n_i \rangle$ only takes the extreme value of 1 or 0. The particle diffusion happens only in the vicinity of the border, where the discontinuous particle density blurs to a “domain-wall region”. Comparing this with the dynamics with the periodic boundary conditions (Fig. 1a), where particles quickly disperse into a homogeneous state, we see the MISE features an anomalous boundary sensitivity. Indeed, the entanglement phases of this generalized monitored system also depend strongly on the boundary conditions. In Fig. 1c, we see that when the system is under periodic boundary conditions, the bipartite entanglement entropy scaling has a log-to-area-law transition, which is typical for a monitored free fermion system. In contrast, there is a single area-law phase for open boundary systems due to MISE, as displayed in Fig. 1d.

To characterize the particle localization, we introduce an extensive local order parameter called the *classical entropy*:

$$S_{\text{cl}} \equiv - \sum_i [\langle n_i \rangle \log \langle n_i \rangle + (1 - \langle n_i \rangle) \log(1 - \langle n_i \rangle)]. \quad (3)$$

We argue this quantity is closely related to MISE since only the nontrivial density (i.e. $\langle n_i \rangle \neq 0, 1$) contributes to S_{cl} . Therefore the asymptotic behavior $S_{\text{cl}} \sim O(1)$ for $L \rightarrow \infty$ implies particle accumulation. In addition, S_{cl} imposes an upper bound for the entanglement entropy. Note that the entanglement entropy satisfies the *subadditivity* [71, 72] $S_{ab} \leq S_a + S_b$ for any two disjoint regions a and b . Consider a bipartite system with subsystems A and B . The subadditivity leads to the entropy inequality $S_A + S_B \leq \sum_i S_i \leq S_{\text{cl}}$, where the last inequality follows from the fact that the eigenvalues of a positive 2×2 matrix majorize [75] the diagonal elements, and thus have less entropy. For a bipartite pure state, $S_A = S_B$, therefore the entanglement entropy of any possible bipartition is bounded by half of the classical entropy: $S_A = S_B \leq S_{\text{cl}}/2$.

In Fig. 2a, we show the time evolution of the classical entropies starting from $|\psi_0\rangle$ under open boundary conditions. The data from the numerical simulation agree

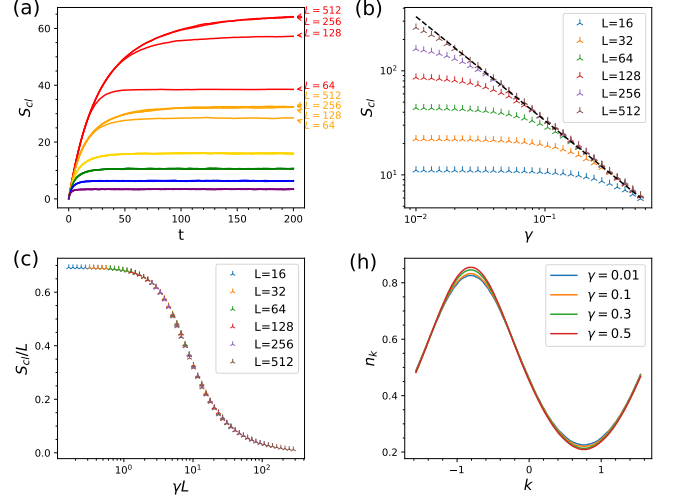


FIG. 2. (a) Time evolution of classical entropy with different measurement rates $\gamma = \{0.05, 0.1, 0.2, 0.3, 0.5, 1.0\}$ and system sizes $L = \{64, 128, 256, 512\}$. The dynamics show no size dependency for $\gamma \geq 0.2$. (b) Classical entropy of steady states with different measurement rates and system sizes. The data point is plotted in the log-log coordinate. In the thermodynamic limit, data approach the line $\log \gamma + \log S_{\text{cl}} \approx 1.2$. (c) Collapsing of classical entropy to the scaling form in Eq. (4). (d) Steady-state particle distribution in momentum space under periodic boundary conditions for $\gamma = \{0.01, 0.1, 0.3, 0.5\}$.

with the “domain-wall developing” picture, which implies when we consider a system larger than the size of the domain-wall region, the evolution $S_{\text{cl}}(t)$ will reach a fixed point. A finer analysis of the dynamics also shows that the system reaches the steady state with characteristic relaxation time $t^* \sim \gamma^{-1}$, the classical entropy for which, as shown in Fig. 2b, has the asymptotic behavior $S_{\text{cl}}(\gamma, L \rightarrow \infty) = c/\gamma$ in the thermodynamic limit. This implies that the characteristic length for the domain wall is $L^* \sim \gamma^{-1}$. The asymptotic behavior, therefore, predicts the area-law entanglement scaling $S \leq c/2\gamma$ for arbitrary L , thus proving the area-law entanglement scaling in the $\gamma \rightarrow 0$ limit.

Moreover, as displayed in Fig. 2c, we observe the steady-state classical entropy has a scale invariance:

$$S_{\text{cl}}(\gamma, L) = Lf(\gamma L), \quad (4)$$

where the scaling function $f(x) \simeq c/x$ in the $x \rightarrow \infty$ limit. For the specific feedback, numerics shows $c \approx 3.3$. Eq. (4) suggests a scale invariance for density profile $n(x)$ in the continuum limit. That is, if we increase the measurement rate by s : $\gamma \rightarrow s\gamma$ and rescale the distance as $x \rightarrow s^{-1}x$, the density profile $n(x)$ will remain the same at interval $[-L/2, L/2]$. For a sufficiently large system: $L \gg L^*$, this simply means $n(x) = \tilde{n}(x)/\gamma$, where $\tilde{n}(x)$ characterizes the shape of the density profile in the domain-wall region, and the constant in the asymptotic limit is related to $\tilde{n}(x)$ by

$$c = \int dx [\tilde{n} \log \tilde{n} + (1 - \tilde{n}) \log(1 - \tilde{n})].$$

The skin effect also manifests as a directional bulk current in the periodic boundary systems. By simulating the system with identical parameters but under periodic boundary conditions, we show in Fig. 2d that there is an imbalance in the momentum distribution even for the $\gamma \ll 1$ case. We can characterize such imbalance by the current: $J[n_k] \equiv \int_{-\pi}^{\pi} v_k n_k dk$, where in the $\gamma \ll 1$ limit, we can approximate the velocity by the dispersion of free Hamiltonian: $v_k \simeq \partial_k E(k) = \sin(k)$. For $\gamma = 0.01$ case, $J \approx -0.94$. The nonzero current suggest the skin effect under open boundary condition.

In the above analysis, we consider only the $\theta = \pi$ case in the feedback operator, while similar MISE appears for arbitrary θ . In the Supplemental Material [60], we show the numerical results for $\theta \neq \pi$. The length of the domain wall, however, is minimized at $\theta = \pi$. When θ approaches zero, we expect that the MISE still appears, although with a large domain wall that may exceed the numerical simulation capability. Therefore, for the projector P_i , arbitrary measurement feedback can result in an extreme boundary sensitivity due to MISE. Besides, readers may wonder whether MISE comes from such a peculiar form of the projectors $\{P_i\}$ since they do not all commute with one another and are not onsite. In the Supplemental Material [60], we present a closely related monitored model where the monitored observable is the onsite particle occupation.

Interacting system.— In the following, we demonstrate that MISE persists in the interacting system. We will focus on the Hamiltonian with nearest-neighbor density-density interaction: $H = \sum_i (c_i^\dagger c_{i+1} + c_{i+1}^\dagger c_i + g n_i n_{i+1})$. The continuous monitoring is the same as the free fermion case (with conditional feedback $U_i = e^{i\pi n_{i+1}}$). We note that previously, the MIPT for the interacting system usually appears on the quantum circuit system with projective measurements, while here, we consider the systems under continuous monitoring. As displayed in Fig. 3a, for the periodic boundary monitored system, the entanglement scaling features a crossing at the critical value $\gamma_c \approx 0.14$, which implies an underneath MIPT. However, for open boundary systems, numerical simulation of a typical dynamical trajectory (Fig. 3b) indicates a similar skin effect as the free systems.

In the presence of MISE, the only active part of the dynamics is the formation and fluctuation of the domain wall. The area-law entanglement entropy due to MISE enables us to efficiently represent the states as the matrix-product states [76, 77] and simulate the time evolution for large system sizes using the TEBD algorithm [78, 79]. Based on the observation of the free fermion systems, we speculate that the classical entropy, and thus the entanglement entropy, $S \propto \gamma^{-1}$. This suggests that a matrix product state with bond dimension $\chi \sim O(e^{1/\gamma})$ is sufficient to describe the state. Besides the trajectory-

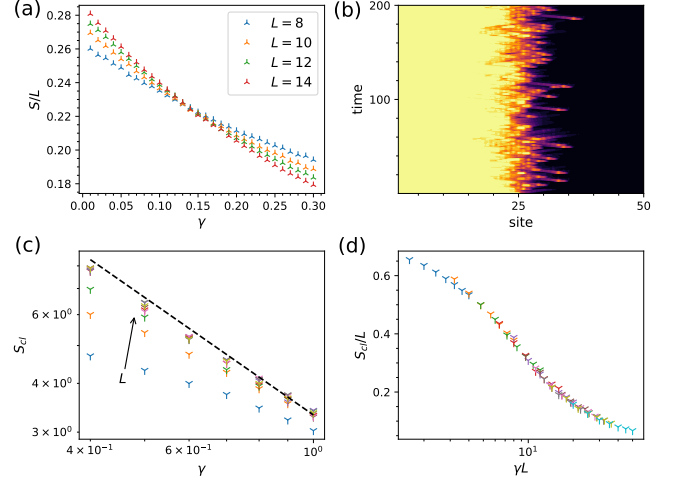


FIG. 3. (a) Steady-state entanglement entropy density S/L of monitored interacting periodic boundary fermion chain for different γ 's, where the coupling constant is $g = 1.0$. The finite size result is obtained by exact diagonalization, and the data crossing at $\gamma_c \simeq 0.14$ indicates an entanglement transition. (b) A trajectory of a monitored system ($L = 50, \gamma = 0.4$) under open boundary conditions. The active part is at the boundary of two frozen domains. (c) Steady-state classical entropy for monitored fermion chain under open boundary conditions. The interacting coupling constant is $g = 1.0$, and the data points are chosen at $\gamma = \{0.4, 0.5, 0.6, 0.7, 0.8, 0.9, 1.0\}$, $L = \{8, 12, 16, 20, 24, 28, 32, 36, 50\}$ (L increases along the arrow). The large-size limit of the data is the line $\log \gamma + \log S_{cl} \approx 1.2$. (d) Data collapsing of classical entropies in the form of Eq. (4).

averaging method, we can also simulate the density evolution under the Lindblad equation by representing the density matrices as matrix-product operators.

We calculate the steady-state classical entropy for different γ , with system size L up to 50 (see Fig. 3c). The numerics shows that at least for $\gamma > 0.4$, the classical entropy satisfies the similar scaling law: $S_{cl}(\gamma, L \rightarrow \infty) \rightarrow c'/\gamma$. This scaling implies the numerical hardness in the small γ regime. Although we are not able to numerically check the scaling behavior in the small γ limit, from the finite size simulation, we obtain the same scaling law as in Eq. (4) (as displayed in Fig. 3d). This implies that even for tiny γ , when $L \gg \gamma^{-1}$, the density of classical entropy S_{cl}/L , and thus the entanglement entropy S/L , approaches zero, excluding a volume-law entangled phase.

Discussion.— In this work, we consider the effect of generalized monitoring on the entanglement phase transition. The appearance of the skin effect in certain open boundary monitored systems qualitatively changes the entanglement structure of the nonequilibrium steady state, resulting in a single area-law phase. We also demonstrate, by varying the parameters of feedback operations, that the MISE is not a fine-tuned phenomenon.

At least for certain projective monitoring, a generic feedback operator will disturb the balance of particle distribution; the presence of an extensive number of such feedback operators thus causes particle accumulation. The MISE suggests that introducing conditional feedback may enrich the entanglement phase structure.

Besides, MISE also provides a novel many-body version of the skin effect of its own interest. Due to the entanglement suppression, the skin effect can be numerically simulated efficiently. Experimentally, the monitoring-feedback setup is relevant in the context of open systems or controllable quantum devices; it is then possible to realize a skin effect without the post-selection required for non-Hermitian dynamics.

Note added.— In the middle of this work, we became aware of a recent work [80], which also considers the effect of generalized monitoring in the context of MIPT. The two works are complementary to each other: in Ref. [80], the authors utilize the feedback (pre-selection) to reveal MIPT as a quantum absorbing state transition that can be directly detected, while our work shows that the presence of conditional feedback may also eliminate the MIPT.

J.R. thanks Chenguang Liang for the valuable discussions. The numerical simulations based on tensor-network use the `ITensor` package [81].

* cfang@iphy.ac.cn

† jieren@iphy.ac.cn

- [1] Y. Li, X. Chen, and M. P. A. Fisher, Quantum zeno effect and the many-body entanglement transition, *Phys. Rev. B* **98**, 205136 (2018).
- [2] B. Skinner, J. Ruhman, and A. Nahum, Measurement-induced phase transitions in the dynamics of entanglement, *Phys. Rev. X* **9**, 031009 (2019).
- [3] A. Chan, R. M. Nandkishore, M. Pretko, and G. Smith, Unitary-projective entanglement dynamics, *Phys. Rev. B* **99**, 224307 (2019).
- [4] Y. Li, X. Chen, and M. P. A. Fisher, Measurement-driven entanglement transition in hybrid quantum circuits, *Phys. Rev. B* **100**, 134306 (2019).
- [5] L. Fidkowski, J. Haah, and M. B. Hastings, How Dynamical Quantum Memories Forget, *Quantum* **5**, 382 (2021).
- [6] A. Nahum, S. Roy, B. Skinner, and J. Ruhman, Measurement and entanglement phase transitions in all-to-all quantum circuits, on quantum trees, and in landau-ginsburg theory, *PRX Quantum* **2**, 010352 (2021).
- [7] M. Ippoliti, M. J. Gullans, S. Gopalakrishnan, D. A. Huse, and V. Khemani, Entanglement phase transitions in measurement-only dynamics, *Phys. Rev. X* **11**, 011030 (2021).
- [8] M. P. A. Fisher, V. Khemani, A. Nahum, and S. Vijay, *Random quantum circuits* (2022).
- [9] Y. Li, X. Chen, A. W. W. Ludwig, and M. P. A. Fisher, Conformal invariance and quantum nonlocality in critical hybrid circuits, *Phys. Rev. B* **104**, 104305 (2021).
- [10] X. Chen, Y. Li, M. P. A. Fisher, and A. Lucas, Emergent conformal symmetry in nonunitary random dynamics of free fermions, *Phys. Rev. Research* **2**, 033017 (2020).
- [11] A. Zabalo, M. J. Gullans, J. H. Wilson, S. Gopalakrishnan, D. A. Huse, and J. H. Pixley, Critical properties of the measurement-induced transition in random quantum circuits, *Phys. Rev. B* **101**, 060301(R) (2020).
- [12] A. Chan, A. De Luca, and J. T. Chalker, Solution of a minimal model for many-body quantum chaos, *Phys. Rev. X* **8**, 041019 (2018).
- [13] A. Nahum, S. Vijay, and J. Haah, Operator spreading in random unitary circuits, *Phys. Rev. X* **8**, 021014 (2018).
- [14] C. W. von Keyserlingk, T. Rakovszky, F. Pollmann, and S. L. Sondhi, Operator hydrodynamics, otocs, and entanglement growth in systems without conservation laws, *Phys. Rev. X* **8**, 021013 (2018).
- [15] T. Zhou and A. Nahum, Emergent statistical mechanics of entanglement in random unitary circuits, *Phys. Rev. B* **99**, 174205 (2019).
- [16] M. P. A. Fisher, V. Khemani, A. Nahum, and S. Vijay, *Random quantum circuits* (2022).
- [17] O. Alberton, M. Buchhold, and S. Diehl, Entanglement transition in a monitored free-fermion chain: From extended criticality to area law, *Phys. Rev. Lett.* **126**, 170602 (2021).
- [18] X. Cao, A. Tilloy, and A. D. Luca, Entanglement in a fermion chain under continuous monitoring, *SciPost Phys.* **7**, 024 (2019).
- [19] M. Coppola, E. Tirrito, D. Karevski, and M. Collura, Growth of entanglement entropy under local projective measurements, *Phys. Rev. B* **105**, 094303 (2022).
- [20] F. Carollo and V. Alba, *Entangled multiplets and unusual spreading of quantum correlations in a continuously monitored tight-binding chain* (2022).
- [21] X. Turkeshi, A. Biella, R. Fazio, M. Dalmonte, and M. Schiró, Measurement-induced entanglement transitions in the quantum ising chain: From infinite to zero clicks, *Phys. Rev. B* **103**, 224210 (2021).
- [22] A. Biella and M. Schiró, Many-Body Quantum Zeno Effect and Measurement-Induced Subradiance Transition, *Quantum* **5**, 528 (2021).
- [23] T. Müller, S. Diehl, and M. Buchhold, Measurement-induced dark state phase transitions in long-ranged fermion systems, *Phys. Rev. Lett.* **128**, 010605 (2022).
- [24] T. Minato, K. Sugimoto, T. Kuwahara, and K. Saito, Fate of measurement-induced phase transition in long-range interactions, *Phys. Rev. Lett.* **128**, 010603 (2022).
- [25] M. Buchhold, Y. Minoguchi, A. Altland, and S. Diehl, Effective theory for the measurement-induced phase transition of dirac fermions, *Phys. Rev. X* **11**, 041004 (2021).
- [26] B. Ladewig, S. Diehl, and M. Buchhold, Monitored open fermion dynamics: Exploring the interplay of measurement, decoherence, and free hamiltonian evolution, *Phys. Rev. Research* **4**, 033001 (2022).
- [27] X. Turkeshi, L. Piroli, and M. Schiró, Enhanced entanglement negativity in boundary-driven monitored fermionic chains, *Phys. Rev. B* **106**, 024304 (2022).
- [28] A. Lavasani, Y. Alavirad, and M. Barkeshli, Measurement-induced topological entanglement transitions in symmetric random quantum circuits, *Nature Physics* **17**, 342 (2021).
- [29] M. Ippoliti, M. J. Gullans, S. Gopalakrishnan, D. A. Huse, and V. Khemani, Entanglement phase transitions in measurement-only dynamics, *Phys. Rev. X* **11**, 011030 (2021).

- (2021).
- [30] R. Vasseur, A. C. Potter, Y.-Z. You, and A. W. W. Ludwig, Entanglement transitions from holographic random tensor networks, *Phys. Rev. B* **100**, 134203 (2019).
 - [31] J. Lopez-Piqueres, B. Ware, and R. Vasseur, Mean-field entanglement transitions in random tree tensor networks, *Phys. Rev. B* **102**, 064202 (2020).
 - [32] C.-M. Jian, B. Bauer, A. Keselman, and A. W. W. Ludwig, [Criticality and entanglement in non-unitary quantum circuits and tensor networks of non-interacting fermions](#) (2020).
 - [33] Z.-C. Yang, Y. Li, M. P. A. Fisher, and X. Chen, Entanglement phase transitions in random stabilizer tensor networks, *Phys. Rev. B* **105**, 104306 (2022).
 - [34] S. Choi, Y. Bao, X.-L. Qi, and E. Altman, Quantum error correction in scrambling dynamics and measurement-induced phase transition, *Phys. Rev. Lett.* **125**, 030505 (2020).
 - [35] M. J. Gullans and D. A. Huse, Scalable probes of measurement-induced criticality, *Phys. Rev. Lett.* **125**, 070606 (2020).
 - [36] M. J. Gullans and D. A. Huse, Dynamical purification phase transition induced by quantum measurements, *Phys. Rev. X* **10**, 041020 (2020).
 - [37] M. J. Gullans, S. Krastanov, D. A. Huse, L. Jiang, and S. T. Flammia, Quantum coding with low-depth random circuits, *Phys. Rev. X* **11**, 031066 (2021).
 - [38] A. J. Daley, Quantum trajectories and open many-body quantum systems, *Advances in Physics* **63**, 77 (2014), <https://doi.org/10.1080/00018732.2014.933502>.
 - [39] Y. Bao, S. Choi, and E. Altman, Theory of the phase transition in random unitary circuits with measurements, *Phys. Rev. B* **101**, 104301 (2020).
 - [40] C.-M. Jian, Y.-Z. You, R. Vasseur, and A. W. W. Ludwig, Measurement-induced criticality in random quantum circuits, *Phys. Rev. B* **101**, 104302 (2020).
 - [41] Y. Li and M. P. A. Fisher, Statistical mechanics of quantum error correcting codes, *Phys. Rev. B* **103**, 104306 (2021).
 - [42] Y. Li, R. Vasseur, M. P. A. Fisher, and A. W. W. Ludwig, [Statistical mechanics model for clifford random tensor networks and monitored quantum circuits](#) (2021).
 - [43] X. Turkeshi, M. Dalmonte, R. Fazio, and M. Schirò, Entanglement transitions from stochastic resetting of non-hermitian quasiparticles, *Phys. Rev. B* **105**, L241114 (2022).
 - [44] M. Ippoliti and V. Khemani, Postselection-free entanglement dynamics via spacetime duality, *Phys. Rev. Lett.* **126**, 060501 (2021).
 - [45] M. Ippoliti, T. Rakovszky, and V. Khemani, Fractal, logarithmic, and volume-law entangled nonthermal steady states via spacetime duality, *Phys. Rev. X* **12**, 011045 (2022).
 - [46] T. Iadecola, S. Ganeshan, J. H. Pixley, and J. H. Wilson, [Dynamical entanglement transition in the probabilistic control of chaos](#) (2022).
 - [47] G. Kells, D. Meidan, and A. Romito, [Topological transitions with continuously monitored free fermions](#) (2021).
 - [48] X. Turkeshi and M. Schirò, [Entanglement and correlation spreading in non-hermitian spin chains](#) (2022).
 - [49] S.-K. Jian, Z.-C. Yang, Z. Bi, and X. Chen, Yang-lee edge singularity triggered entanglement transition, *Phys. Rev. B* **104**, L161107 (2021).
 - [50] K. Kawabata, T. Numasawa, and S. Ryu, [Entanglement phase transition induced by the non-hermitian skin effect](#) (2022).
 - [51] S. Gopalakrishnan and M. J. Gullans, Entanglement and purification transitions in non-hermitian quantum mechanics, *Phys. Rev. Lett.* **126**, 170503 (2021).
 - [52] S. Yao and Z. Wang, Edge states and topological invariants of non-hermitian systems, *Phys. Rev. Lett.* **121**, 086803 (2018).
 - [53] V. M. Martinez Alvarez, J. E. Barrios Vargas, and L. E. F. Foa Torres, Non-hermitian robust edge states in one dimension: Anomalous localization and eigenspace condensation at exceptional points, *Phys. Rev. B* **97**, 121401(R) (2018).
 - [54] K. Zhang, Z. Yang, and C. Fang, Correspondence between winding numbers and skin modes in non-hermitian systems, *Phys. Rev. Lett.* **125**, 126402 (2020).
 - [55] K. Yokomizo and S. Murakami, Non-bloch band theory of non-hermitian systems, *Phys. Rev. Lett.* **123**, 066404 (2019).
 - [56] N. Okuma, K. Kawabata, K. Shiozaki, and M. Sato, Topological origin of non-hermitian skin effects, *Phys. Rev. Lett.* **124**, 086801 (2020).
 - [57] Z. Yang, K. Zhang, C. Fang, and J. Hu, Non-hermitian bulk-boundary correspondence and auxiliary generalized brillouin zone theory, *Phys. Rev. Lett.* **125**, 226402 (2020).
 - [58] D. S. Borgnia, A. J. Kruchkov, and R.-J. Slager, Non-hermitian boundary modes and topology, *Phys. Rev. Lett.* **124**, 056802 (2020).
 - [59] L. E. F. F. Torres, Perspective on topological states of non-hermitian lattices, *Journal of Physics: Materials* **3**, 014002 (2019).
 - [60] See Supplemental Material for detail regarding the stochastic Schrödinger Equation, the uniqueness of nonequilibrium steady state, free fermion simulation, monitored free fermion with different conditional feedback, and the additional generalized monitored model.
 - [61] K. Jacobs and D. A. Steck, A straightforward introduction to continuous quantum measurement, *Contemporary Physics* **47**, 279 (2006), <https://doi.org/10.1080/00107510601101934>.
 - [62] H. M. Wiseman and G. J. Milburn, *Quantum Measurement and Control* (Cambridge University Press, 2009).
 - [63] A. Barchielli and M. Gregoratti, The stochastic schrödinger equation, in *Quantum Trajectories and Measurements in Continuous Time: The Diffusive Case* (Springer Berlin Heidelberg, Berlin, Heidelberg, 2009) pp. 11–49.
 - [64] G. Lindblad, On the generators of quantum dynamical semigroups, *Communications in Mathematical Physics* **48**, 119 (1976).
 - [65] E. B. Davies, Markovian master equations, *Communications in Mathematical Physics* **39**, 91 (1974).
 - [66] H.-P. Breuer and F. Petruccione, *The Theory of Open Quantum Systems* (Oxford University Press, 2007).
 - [67] D. E. Evans, Irreducible quantum dynamical semigroups, *Communications in Mathematical Physics* **54**, 293 (1977).
 - [68] A. Frigerio, Stationary states of quantum dynamical semigroups, *Communications in Mathematical Physics* **63**, 269 (1978).
 - [69] H. Spohn, Kinetic equations from hamiltonian dynamics: Markovian limits, *Rev. Mod. Phys.* **52**, 569 (1980).
 - [70] T. Prosen, Matrix product solutions of boundary driven

- quantum chains, *Journal of Physics A: Mathematical and Theoretical* **48**, 373001 (2015).
- [71] M. A. Nielsen and I. L. Chuang, *Quantum Computation and Quantum Information: 10th Anniversary Edition* (Cambridge University Press, 2010).
 - [72] M. M. Wilde, *Quantum Information Theory* (Cambridge University Press, 2013).
 - [73] S. Bravyi, Lagrangian representation for fermionic linear optics [10.48550/ARXIV.QUANT-PH/0404180](https://arxiv.org/abs/10.48550/ARXIV.QUANT-PH/0404180) (2004).
 - [74] N. Hatano and D. R. Nelson, Localization transitions in non-hermitian quantum mechanics, *Phys. Rev. Lett.* **77**, 570 (1996).
 - [75] R. A. Horn and C. R. Johnson, *Topics in Matrix Analysis* (Cambridge University Press, 1991).
 - [76] M. Fannes, B. Nachtergaele, and R. F. Werner, Finitely correlated states on quantum spin chains, *Communications in Mathematical Physics* **144**, 443 (1992).
 - [77] M. W. J. C. D. Perez-Garcia, F. Verstraete, Matrix product state representations (2007), [arXiv:quant-ph/0608197](https://arxiv.org/abs/quant-ph/0608197).
 - [78] G. Vidal, Efficient classical simulation of slightly entangled quantum computations, *Phys. Rev. Lett.* **91**, 147902 (2003).
 - [79] G. Vidal, Classical simulation of infinite-size quantum lattice systems in one spatial dimension, *Phys. Rev. Lett.* **98**, 070201 (2007).
 - [80] M. Buchhold, T. Müller, and S. Diehl, *Revealing measurement-induced phase transitions by pre-selection* (2022).
 - [81] M. Fishman, S. R. White, and E. M. Stoudenmire, The ITensor software library for tensor network calculations (2020), [arXiv:2007.14822](https://arxiv.org/abs/2007.14822).

Supplemental Material for “Absence of entanglement transition due to measurement-induced skin effect”

STOCHASTIC SCHRÖDINGER EQUATION

Microscopically, a measurement process involves a short-time interaction between the system and the probe, which are initially separable:

$$|\psi_{AB}\rangle = e^{-iH_{\text{int}}\Delta t}|\psi_A\rangle \otimes |\psi_B\rangle, \quad (5)$$

where the wave function of the measured system is denoted as $|\psi_A\rangle$ and the probe $|\psi_B\rangle$. When Δt is much smaller than the time scale of the system, the system can be regarded as static during the measurement. Such measurement is called the *strong measurement*. The probe is thought to be a device that can convert quantum information to the classical one, which takes the form of standard projective measurement. That is, suppose the eigenbasis of the probe is $\{|\phi_n\rangle\}$, the probability of getting a record n is

$$p_n = \langle \phi_n | \rho_B | \phi_n \rangle, \quad \rho_B \equiv \text{Tr}_A |\psi_{AB}\rangle \langle \psi_{AB}|, \quad (6)$$

and the feedback of the measurement to the system is

$$|\tilde{\psi}_A^{(n)}\rangle = \langle \phi_n | e^{-iH_{\text{int}}\Delta t} |\psi_A\rangle \otimes |\psi_B\rangle \equiv M_n |\psi_A\rangle. \quad (7)$$

The completeness condition requires

$$\sum_n \langle \tilde{\psi}_A^{(n)} | \tilde{\psi}_A^{(n)} \rangle = 1 \implies \sum_n M_n^\dagger M_n = 1. \quad (8)$$

This is the general form of the measure. In the language of density operator, a measurement is described by a set of operators $\{M_n\}$. A measurement process may record a result n with probability p_n and change the state to:

$$\rho \rightarrow \frac{M_n \rho M_n^\dagger}{\|M_n \rho M_n^\dagger\|}. \quad (9)$$

If the measurement result is not known, the averaged density matrix after the measurement is

$$\rho \rightarrow \sum_n M_n \rho M_n^\dagger. \quad (10)$$

Such a map is called the quantum channel [71].

On the other hand, if the strength of system-probe coupling is comparable with the energy scale of the system, which is the case for an open quantum system, the quantum channel expression should depend on time Δt . This kind of measurement process is called *weak measurement*. When the system is *Markovian* (the equation of motion depends only on the near past), the course-grained dissipation process can be described by the channel:

$$M_n = L_n \sqrt{\gamma \Delta t}, \quad M_0 = \sqrt{1 - \sum_{n>0} M_n^\dagger M_n} = 1 - \frac{\gamma}{2} \sum_{n>0} L_n^\dagger L_n \Delta t + O(\Delta t^2). \quad (11)$$

For the density matrix, the coarse-grained differential equation is the Lindblad equation:

$$\frac{d\rho}{dt} = \lim_{\Delta t \rightarrow 0} \frac{1}{\Delta t} \sum_n M_n e^{-iH\Delta t} \rho e^{iH\Delta t} M_n^\dagger = -i[H, \rho] - \frac{\gamma}{2} \sum_i \{L_i^\dagger L_i, \rho\} + \gamma \sum_i L_i \rho L_i^\dagger. \quad (12)$$

The joint dynamics of Hamiltonian evolution and measurement can be equivalently described by the stochastic process, as shown in Fig. 4, where for each time step Δt , the system first undergoes a coherent evolution $|\psi\rangle \rightarrow e^{-iH\Delta t}|\psi\rangle$, then the application of measurement produces a random process:

$$|\psi\rangle \rightarrow \begin{cases} M_n(\Delta t)|\psi\rangle & P_n = \langle \psi | L_n^\dagger L_n | \psi \rangle \gamma \Delta t \\ M_0(\Delta t)|\psi\rangle & P_0 = 1 - \sum_{n>0} P_n \end{cases}. \quad (13)$$

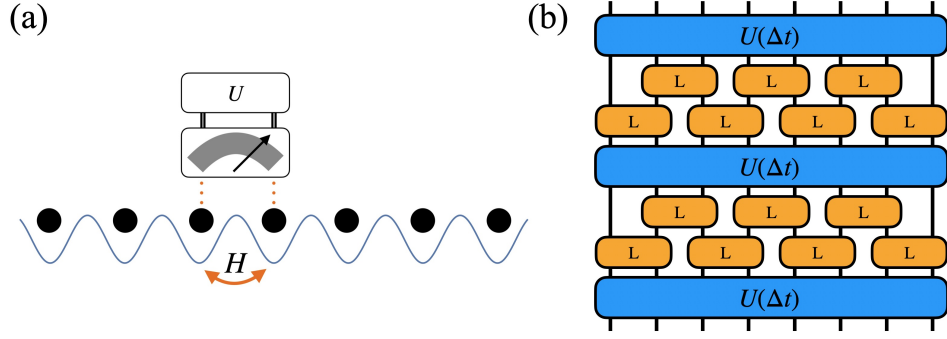


FIG. 4. (a) Schematic of a fermion chain under nearest neighbor interaction and generalized monitoring on each pair of neighboring sites. Unitary feedback will be applied if the probe records a quantum jump. (b) Circuits representation of the discretized Hamiltonian evolution with constant monitoring.

Different records of the measurement result correspond to different trajectories, and the Lindblad equation is equivalent to the trajectory averaged of such stochastic processes. In the continuum limit, the stochastic differential equation can be formulated by introducing a Poisson random variable dW_n taking the discrete values of 0 or 1. The $dW_n = 1$ case corresponds to registering a quantum jump, otherwise, $dW_n = 0$. The expectation value for random dW_n is proportional to dt :

$$\overline{dW_n} = \langle \psi | L_n^\dagger L_n | \psi \rangle \gamma dt. \quad (14)$$

Different dW_n 's are independent, i.e., they satisfy the orthogonal condition

$$dW_m dW_n = \delta_{mn} dW_m. \quad (15)$$

Therefore, the random quantum jump process $|\psi\rangle \rightarrow M_n |\psi\rangle$ is described by the expression

$$d|\psi\rangle = \left(\frac{L_n}{\sqrt{\langle L_n^\dagger L_n \rangle}} - 1 \right) |\psi\rangle dW_n, \quad (16)$$

and the null-detection case correspond to $|\psi\rangle \rightarrow M_0 |\psi\rangle$, which is described by a non-Hermitian differential equation:

$$d|\psi\rangle = -\frac{\gamma}{2} \sum_m (L_m^\dagger L_m - \langle L_m^\dagger L_m \rangle) |\psi\rangle dt, \quad (17)$$

where the $\langle L_m^\dagger L_m \rangle$ is introduced for the normalization purpose. Together with the coherent evolution, we obtain the stochastic Schrödinger equation in the main text:

$$d|\psi\rangle = -iH_{\text{eff}} |\psi\rangle dt + \sum_m \left(\frac{L_m}{\sqrt{\langle L_m^\dagger L_m \rangle}} - 1 \right) |\psi\rangle dW_m. \quad (18)$$

For numerical simulation of Eq. (18), we can first discretize the time into small interval Δt . The discrete evolution is then

$$|\psi(t + \Delta t)\rangle = \mathcal{M}_{\Delta t} [e^{-iH_{\text{eff}} \Delta t} |\psi(t)\rangle], \quad (19)$$

where $\mathcal{M}_{\Delta t}$ represents the quantum jump that randomly happened in time interval Δt :

$$\mathcal{M}_{\Delta t} [|\psi\rangle] \propto \prod_{m \in I} L_m |\psi\rangle. \quad (20)$$

In the Eq. (20), the set I denotes the random jump processes, which can be obtained by

$$I = \{n | r_n < \gamma \langle L_n^\dagger L_n \rangle \Delta t\}, \quad (21)$$

where $\{r_n \in (0, 1)\}$ is a set of independent random variables with evenly distributed probability.

UNIQUENESS OF NONEQUILIBRIUM STEADY STATE

In Refs. [67, 68] (see review in Ref. [69] and application in Ref. [70]), it was shown that a Lindblad equation has unique nonequilibrium steady state if and only if the set

$$\{H, L_1, L_1^\dagger, L_2, L_2^\dagger, \dots\} \quad (22)$$

generates (under multiplication and addition) the complete algebra on the Hilbert space. The general proof assumes no conserved quantity for the Lindblad equation. For the particle number conserving case, as we considered in the main text, we can focus on the Hilbert subspace \mathcal{H}_N spanned by N -particle states. The uniqueness condition then says if $\{H, L_1, L_1^\dagger, L_2, L_2^\dagger, \dots\}$ generates the complete algebra on \mathcal{H}_N , the steady state in \mathcal{H}_N will be unique.

We first prove that the Hamiltonian (under open boundary conditions)

$$H = \sum_i (c_i^\dagger c_{i+1} + c_{i+1}^\dagger c_i) \quad (23)$$

and the projectors

$$P_i = \frac{1}{2}(c_i^\dagger - ic_{i+1}^\dagger)(c_i + ic_{i+1}) \quad (24)$$

generate the whole algebra. Note H and P_1, P_2 together generate the following particle number operators:

$$\begin{aligned} n_1 - n_3 &= P_2 - P_1 + i[H, P_1 + P_2], \\ n_1 + n_2 &= \frac{1}{2}(P_1 + P_2 + i[H, n_1 - n_3] + n_1 - n_3), \\ n_2 + n_3 &= (n_1 + n_2) - (n_1 - n_3). \end{aligned} \quad (25)$$

Then, some straightforward algebra lead to

$$\begin{aligned} c_1^\dagger c_2 - c_2^\dagger c_1 &= i(n_1 + n_2) - iP_1, \\ c_1^\dagger c_2 + c_2^\dagger c_1 &= [c_1^\dagger c_2 - c_2^\dagger c_1, n_2 + n_3], \\ c_2^\dagger c_3 - c_3^\dagger c_2 &= i(n_2 + n_3) - iP_2, \\ c_2^\dagger c_3 + c_3^\dagger c_2 &= [n_1 + n_2, c_2^\dagger c_3 - c_3^\dagger c_2]. \end{aligned} \quad (26)$$

Upon some addition among Eqs. (26), we obtain the operator $c_1^\dagger c_2$, $c_2^\dagger c_3$ and their Hermitian conjugates. The commutations of them further produce $c_1^\dagger c_3$ and its conjugate. Also, note that

$$[c_1^\dagger c_2, c_2^\dagger c_1] = n_1 - n_2. \quad (27)$$

Together with Eqs. (25), we generate all fermion bilinear terms $c_i^\dagger c_j$ (including $i = j$ case) on sites $(1, 2, 3)$. To proceed, we subtract the hopping terms between sites $(1, 2)$ from H . The resulting operator is equivalent to a shorter chain starting from site 2. We can then utilize the calculation above to obtain all $c_i^\dagger c_j$ terms on sites $(2, 3, 4)$. We eventually obtain all fermion bilinear terms on the chain by applying the strategy iteratively. Note that fermion bilinear terms $c_i^\dagger c_j$ generate the complete algebra within a fixed particle-number sector since any two product states in the sector can be related by applying several fermion hopping terms.

For the generalized monitored system described by the jump operators $\{L_n = U_n P_n\}$, the proof of uniqueness is essentially the same as the projective case. Note that we can generate all P_i terms by multiplying to jump operators

$$P_i = L_i^\dagger L_i. \quad (28)$$

In this way, we can generate the complete operator algebra in the same way as above.

We argue that the completeness of the operator algebra holds for generic open systems since the exact decoupling of Hilbert space is the result of symmetries or fine-tuning. For the interacting system where the Hamiltonian is

$$H = \sum_i (c_i^\dagger c_{i+1} + c_{i+1}^\dagger c_i + g n_i n_{i+1}). \quad (29)$$

The above argument means for a random value of g , we should expect the completeness of the operator algebra. We can also consider the case where the coupling constant is smoothly varying in the space. In particular, let $g_i = 0$ for the sites near the boundary. Following the same procedure, we can generate the operator algebra of the subsystem near the boundary. Assume that we meet the first nonzero g at site $i+1$. It means that we have the complete operator algebra (within fixed filling number) $\mathcal{A}_{[1,i]}$ of the subsystem consisting of sites $1, \dots, i$. We first subtract all terms within $\mathcal{A}_{[1,i]}$ from the Hamiltonian and denote the result as $H_{[i+1,N]}$. Consider the commutators

$$\begin{aligned} [n_{i-1}, H_{[i+1,N]}] &= c_i^\dagger c_{i+1} - c_{i+1}^\dagger c_i, \\ [n_{i-1}, c_i^\dagger c_{i+1} - c_{i+1}^\dagger c_i] &= c_i^\dagger c_{i+1} + c_{i+1}^\dagger c_i. \end{aligned} \quad (30)$$

In this way, we generate the hopping terms $c_i^\dagger c_{i+1}$ and $c_{i+1}^\dagger c_i$. Those terms together with $\mathcal{A}_{[1,i]}$ generate the algebra $\mathcal{A}_{[1,i+1]}$. This procedure can proceed iteratively, therefore producing the complete algebra.

FREE FERMION SIMULATION

The free fermion system can be efficiently represented by the Gaussian state [73]. For a particle number conserving system, the Gaussian state is a quasimode-occupied state, represented by a matrix B :

$$|B\rangle \equiv \prod_{j=1}^N \sum_i B_{ij} c_i^\dagger |0\rangle = \bigotimes_{j=1}^N |B_j\rangle, \quad (31)$$

where each column B_j is an occupied quasimode. Note that there is an $SU(N)$ gauge freedom for the matrix B , i.e.,

$$|B'\rangle = |BU\rangle = |B\rangle, \quad (32)$$

where U is an arbitrary $SU(N)$ matrix. Such gauge freedom implies that a Gaussian state is entirely specified by the linear subspace spanned by the quasimodes B_i 's.

The random Schrödinger equation can be Trotterized as Eq. (19). Using the Baker-Campbell-Hausdor formula $e^A B e^{-A} = e^{\text{ad}_A} B$, the nonunitary evolution is

$$\begin{aligned} e^{-iH_{\text{eff}}\Delta t} |B_t\rangle &= \prod_{j=1}^N \sum_i B_{ij} e^{-iH_{\text{eff}}\Delta t} c_i^\dagger e^{iH_{\text{eff}}\Delta t} |0\rangle = \prod_{j=1}^N \sum_i B_{ij} e^{-i\Delta t[H_{\text{eff}}, \cdot]} c_i^\dagger |0\rangle \\ &= \prod_{j=1}^N \sum_i \sum_k B_{ij} c_k^\dagger [e^{-iH_{\text{eff}}\Delta t}]_{ki} |0\rangle = \prod_{j=1}^N \sum_k [e^{-iH_{\text{eff}}\Delta t} B_{ij}]_{kj} c_k^\dagger |0\rangle \\ &= |e^{-iH_{\text{eff}}\Delta t} B_t\rangle. \end{aligned} \quad (33)$$

That is, the matrix is multiplied by the exponential of the effective non-Hermitian (single-body) Hamiltonian matrix. Note that the resulting matrix is not orthogonal anymore, while the state is still well-defined by the linear space spanned by those unorthogonal vectors. In general, for a Gaussian state represented by matrix B , we can obtain a canonical form for the representing matrix using the QR decomposition $B = Q \cdot R$, where Q is a unitary matrix and R is upper triangular. Note that Q and B span the same linear space, so the Gaussian state can be expressed as $|Q\rangle$.

The supper operator $\mathcal{M}_{\Delta t}$ in Eq. (19) corresponds to the Poisson jump process, where for each index i , we randomly decide whether a quantum jump process

$$|B\rangle \rightarrow \frac{L_i |B\rangle}{\|L_i |B\rangle\|} \quad (34)$$

happens, with the probability

$$p_i = \langle B | L_i^\dagger L_i | B \rangle \gamma \Delta t \quad (35)$$

The L_m 's we choose in the main text have the form

$$L_m = e^{ih} d^\dagger d, \quad d^\dagger = \sum_i a_i c_i^\dagger, \quad h = \sum_{ij} h_{ij} c_i^\dagger c_j, \quad (36)$$

where d^\dagger is a quasimode, and h is a fermion bilinear. The following shows that the Gaussian form is preserved by such jump operator L_m . First, the probability of the jump process is

$$\langle B|L_m^\dagger L_m|B\rangle = \langle B|d^\dagger d|B\rangle = \|d|B\rangle\|^2. \quad (37)$$

The action of annihilation operator d on $|B\rangle$ is

$$d|B\rangle = \sum_k a_k^* c_k \prod_j \sum_i c_i^\dagger B_{ij} |0\rangle = \sum_j \langle a|B_j\rangle \bigotimes_{l \neq j} |B_l\rangle, \quad (38)$$

so we can obtain the probability

$$p_m = \sum_j |\langle a|B_j\rangle|^2 \gamma \Delta t. \quad (39)$$

Besides, we can utilize the gauge freedom to choose the basis such that $\langle a|B'_j\rangle = 0$ for $j > 1$. The matrix B' always exists since we can always find a column j that $\langle a|B_j\rangle \neq 0$ (otherwise, the probability of the jump is zero). We then move the column to the first and define the column as

$$|B'_j\rangle = |B_j\rangle - \frac{\langle a|B_j\rangle}{\langle a|B_1\rangle} |B_1\rangle, \quad j > 1. \quad (40)$$

Note that such column transformation does not alter the linear space B spans, while the orthogonality and the normalization might be affected and should be renormalized afterward. Eq. (38) then simplified to:

$$d|B\rangle = \bigotimes_{j>1} |B'_j\rangle. \quad (41)$$

The result of the quantum jump is

$$L_m|B\rangle = |e^{ih}a\rangle \bigotimes_{j>1} |e^{ih}B'_j\rangle. \quad (42)$$

The representation of the outcome state is also not orthogonal. An additional QR decomposition is needed to convert it to canonical form.

MONITORED FREE FERMION WITH DIFFERENT CONDITIONAL FEEDBACK

In this appendix, we provide more numerical results on the monitored free fermion system with Hamiltonian

$$H = \sum_i (c_i^\dagger c_{i+1} + c_{i+1}^\dagger c_i) \quad (43)$$

and the generalized monitoring described by the operator

$$L_i = \frac{1}{2} e^{i\theta n_{i+1}} (c_i^\dagger - i c_{i+1}^\dagger) (c_i + i c_{i+1}). \quad (44)$$

Apart from the $\theta = \pi$ discussed in the main text, in Fig. 5, we show the numerical simulations on different θ 's. The steady-state classical entropies in the thermodynamic limit $L \rightarrow \infty$ all satisfy the general asymptotic behaviors:

$$S_{\text{cl}}(\gamma, L \rightarrow \infty) = \frac{c(\theta)}{\gamma}, \quad (45)$$

while the constant $c(\theta)$ increases as θ decreases:

θ/π	1	0.9	0.8	0.7	0.6	0.5	0.4	0.3
$\log c(\theta)$	1.2	1.25	1.35	1.5	1.75	2.15	2.8	4

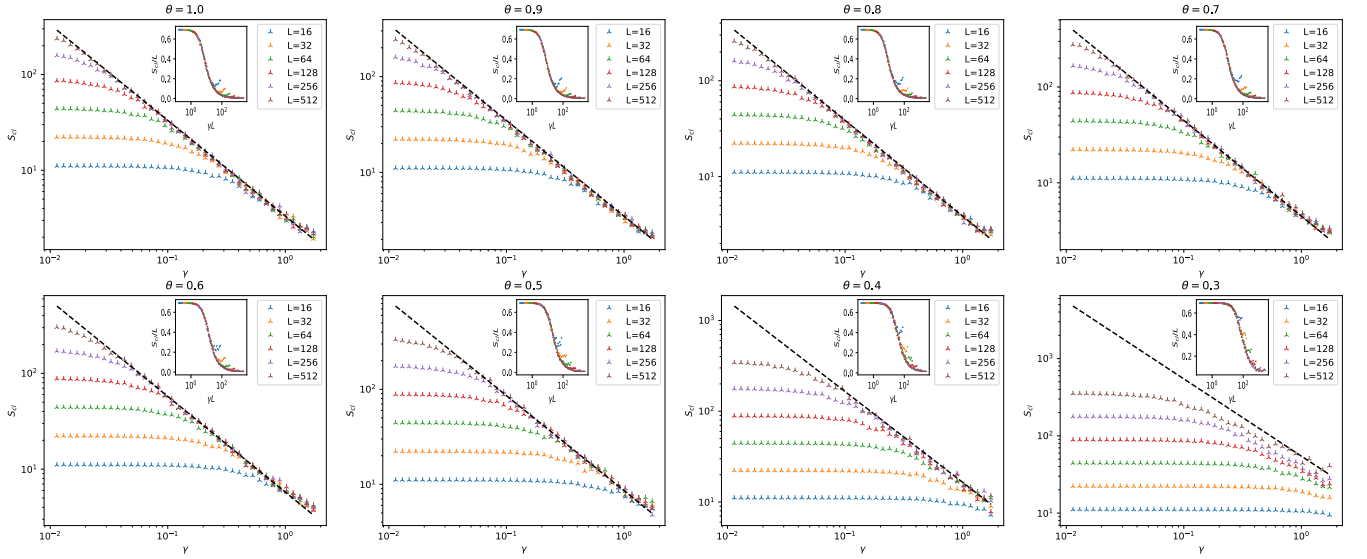


FIG. 5. Steady-state classical entropies for feedback $U_i = \exp(i\theta n_{i+1})$, where we chose θ from π to 0.3π . the data points all approach the asymptotic line $\log \gamma + \log S_{cl} = c(\theta)$ in the thermodynamic limit. Insets: the data collapse into the form Eq. (46) for $\gamma < 1$. For $\gamma > 1$, the data points will deviate from the scaling curve.

As discussed in the main text, the constant $c(\theta)$ determines the spatial extents of the domain wall. The finite data point we obtained implies that $c(\theta)$ increases exponentially fast when $\theta \rightarrow 0$. In the $\theta = 0$ case, $c(\theta)$ diverges and there is no skin effect. The large-size domain walls impose significant overhead for numerical simulations. For small θ ($\leq 0.3\pi$), accessing the thermodynamic limit becomes practically hard.

However, from the insets of Fig. 5, we see that the numerical data ($\gamma < 1$) for different θ 's all collapse into the scaling form

$$S_{cl} = L f_\theta(\gamma L), \quad (46)$$

with the specific scaling function depending on θ . As discussed, Eq. (46) directly implies the skin effect. Based on the numerical results, we speculate the scaling form Eq. (46) holds for different θ and γ . Therefore the skin effect is not a fine-tuned property of the feedback parameters.

ADDITIONAL GENERALIZED MONITORED MODEL

This section presents an additional generalized monitored model closely related to that we investigate in the main text. Firstly, we claim that the skin effect appears for the system with the same Hamiltonian

$$H = \sum_i (c_i^\dagger c_{i+1} + c_{i+1}^\dagger c_i), \quad (47)$$

but under the generalized monitoring described by the projector

$$P_{2i-1} = \frac{1}{2}(c_{2i-1}^\dagger - i c_{2i}^\dagger)(c_{2i-1} + i c_{2i}) \quad (48)$$

followed by feedback $U_{2i-1} = e^{i\pi n_{2i}}$. This model is basically the same as the model in the main text, but the number monitoring is reduced by half, and now the projectors $\{U_{2i-1}\}$ all commute with one another. Because of the monitoring, the unit cell is now enlarged by factor 2. We relabel the fermion operator as $c_{i,A}$ and $c_{i,B}$. The Hamiltonian in the now basis is written as

$$H = \sum_i \left(c_{i,A}^\dagger c_{i,B} + c_{i,B}^\dagger c_{i+1,A} + H.c. \right), \quad (49)$$

the projector is

$$P_i = \frac{1}{2}(c_{i,A}^\dagger - ic_{i,B}^\dagger)(c_{i,A} + ic_{i,B}), \quad (50)$$

and feedback is $U_i = e^{i\pi n_{i,B}}$. We show the evolution of the particle density in Fig. 6a, which clearly shows the skin effect induced by generalized monitoring.

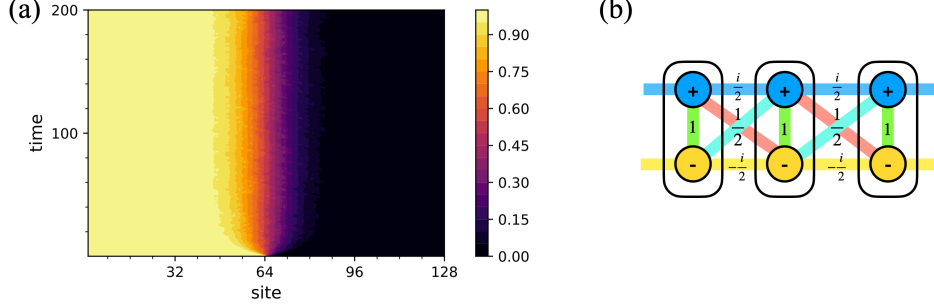


FIG. 6. (a) Density evolution of the monitored system with $\gamma = 0.3$ and $L = 128$, under open boundary conditions. The steady-state displays a similar skin effect as the original one in the main text. (b) Schematic of hopping Hamiltonian Eq. (52).

Now we apply a unitary transformation to the fermion basis:

$$c_{i,+} = \frac{1}{\sqrt{2}}(c_{i,A} + ic_{i,B}), \quad c_{i,-} = \frac{1}{\sqrt{2}}(c_{i,B} + ic_{i,A}) \quad (51)$$

The nearest-neighbor hopping Hamiltonian now becomes a more complicated, but still local hopping free fermion model

$$H = h_0 + h_1 + h_2 + h_3, \quad (52)$$

where $\{h_0, h_1, h_2, h_3\}$ are hopping terms among neighboring unit cells (see Fig. 6b):

$$\begin{aligned} h_0 &= \sum_i (c_{i,+}^\dagger c_{i,-} + c_{i,-}^\dagger c_{i,+}), & h_1 &= \frac{1}{2} \sum_i (c_{i,-}^\dagger c_{i+1,+} + c_{i+1,+}^\dagger c_{i,-}), \\ h_2 &= \frac{i}{2} \sum_i (c_{i,+}^\dagger c_{i+1,+} - c_{i+1,+}^\dagger c_{i,-}), & h_3 &= \frac{1}{2} \sum_i (c_{i,+}^\dagger c_{i+1,-} + c_{i+1,-}^\dagger c_{i,+}). \end{aligned} \quad (53)$$

Under the new basis, the projector becomes an onsite measurement of particle occupation $P_i = n_{i,+}$, and the conditional feedback operator is now

$$U_i = \exp \left[i \frac{\pi}{2} (c_{i,-}^\dagger + ic_{i,+}^\dagger)(c_{i,-} - ic_{i,+}) \right]. \quad (54)$$

The new generalized monitored model consists of a free-hopping Hamiltonian, an onsite measurement, and unitary feedback acting on the unit cell i . Since it is related to the original model by a local unitary transformation, a similar skin effect appears in this model.